Available online at www.eccomasproceedia.org
Eccomas Proceedia UNCECOMP (2017) 350-371

ECCOMAS
Proceedia

UNCECOMP 2017
2nd ECCOMAS Thematic Conference on
Uncertainty Quantification in Computational Sciences and Engineering
M. Papadrakakis, V. Papadopoulos, G. Stefanou (eds.)
Rhodes Island, Greece, 15–17 June 2017

A BAYESIAN APPROACH TO MODEL CALIBRATION AND PARAMETER ESTIMATION IN POTENTIAL DROP MEASURING

Thomas Berg[1], **Sven von Ende**[2] **and Rolf Lammering**[1]

[1]Institute of Mechanics, Helmut Schmidt University/University of the Federal Armed Forces Hamburg
Holstenhofweg 85, 22043 Hamburg, GERMANY
e-mail: {thomas.berg, rolf.lammering}@hsu-hh.de

[2]Rolls-Royce Deutschland Ltd & Co KG
Eschenweg 11, Dahlewitz, 15827 Blankenfelde-Mahlow, GERMANY
e-mail: sven.vonende@rolls-royce.com

Keywords: Probabilistic analysis, Fatigue crack growth, Fatigue test methods, Bayesian model calibration, Parameter estimation.

Abstract. *The direct current potential drop method is a widespread technique used to monitor fatigue-related crack initiation and growth. However, to determine the size of cracks in a structure indirectly via potential drop measurements in the presence of unknown material-dependent parameters bears not only the challenge of model calibration but of parameter estimation as well.*

A solution to this inverse problem is accomplished by a Bayesian approach. Therefore, physics and measuring characterising models as well as prior information on the unknown crack size and unknown parameters are specified. Within this thus defined probabilistic state space model, Bayesian inference is performed to infer the crack size of fatigue-tested specimens from potential drop measurements while taking into account persistent variabilities and uncertainties. The results obtained in the form of joint conditional posterior distributions are utilised to calibrate the potential drop measuring and to estimate the unknown parameters on the one hand as well as to estimate the crack size on the other hand. By comparison with experimentally acquired actual crack size data, the proposed Bayesian approach is found to yield accurate results, rendering the methodology highly promising.

Peer-review under responsibility of the organizing committee of UNCECOMP 2017.
doi: 10.7712/120217.5375.17094

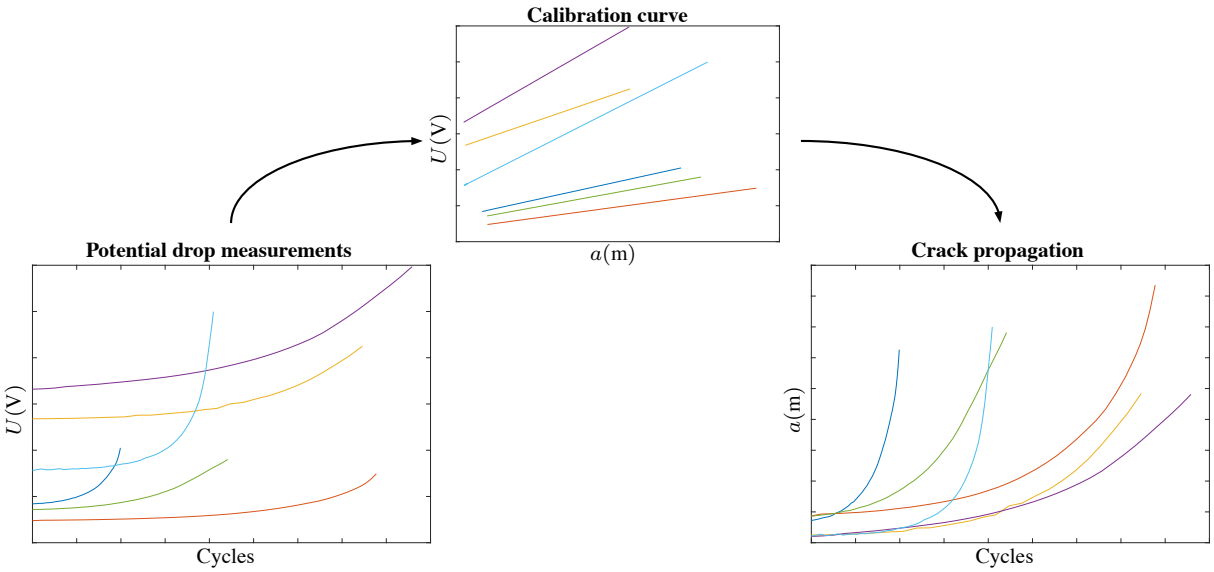

Figure 1: Direct current potential drop method: The initially unknown relation between potential drop U and crack size a is utilised to determine the crack propagation path a over cycles N.

1 INTRODUCTION

Within the *direct current potential drop* (DCPD) method, the difference in electric potential between two points with an intermediate defect is measured. Considering a crack or corrosion as the defect, the measurements can be utilised to obtain accurate information about the shape and size in situ without the necessity of optical assessment, constituting the DCPD method as widely accepted approach to non-destructive testing in aviation, civil engineering, petrochemical and power generation industries [1]. Monitoring fatigue-related crack initiation and growth, a main challenge in applying DCPD measuring lies in facilitating a linkage between the observed potential drop and the underlying crack geometry, e.g. the crack size. However, the linkage between both quantities can be accomplished by a calibration curve as conceptually shown in Figure 1. A new methodology to address this problem by Bayesian filtering and smoothing has been presented in [2] and is carried on and enhanced with the present contribution.

The various ways to obtain calibration curves encompass experimental, analytical and numerical approaches: By means of manually introduced and pre-defined defects, a reference test serves as experimental calibration for subsequent specimens with a consistent probe and electrode setup [3]. In other experimental approaches, crack front marking techniques like heat tints [4] and beachmarks (frequency or stress ratio shifts) [5,6] can be either utilised to allow a reference-based calibration as well or, when accepting the loss of the specimen, be harnessed for a specific calibration subsequent to the test. By solving the Laplace equation of an electrical potential for certain geometry and boundary conditions, theoretical calibrations can be derived. Though this is not generally applicable, [7] provides analytical solutions for simple geometries like plane single-edge, double-edge and centre cracks. For more complex geometries numerical methods like FEM have been employed [8,9].

The challenge of obtaining a calibration curve can be ascribed to finding a solution to the inverse problem of deriving unobservable states from a set of observations and can be reasonably addressed by a Bayesian approach [10]. Bayesian inference has been widely used in

model-based structural health monitoring and prognostics in the context of damage diagnosis and damage prognosis, where sensor data of any kind is used in conjunction with physics and measuring characterising models to assess the state of a single component or a whole structure while taking into account system-inherent uncertainties and variabilities, e.g. [11, 12]. In the presence of unknown parameters that govern the physics-based models, for example parameters of a damage evolution model, the inverse problem becomes even more complex.

Herein, the model calibration challenge in DCPD measuring is addressed in conjunction with parameter estimation by a Bayesian approach for fatigue-tested corner crack specimens. As opposed to [2] where solely the model calibration and state estimation is dealt with, the recursive Bayesian filtering and smoothing framework is extended to additionally infer the unknown dynamic model parameters from the cycle-dependent potential drop observations. Furthermore, two different dynamic models that depict the underlying physical process with diverging precision are utilised. As a consequence, neither are marking techniques and the accompanying destruction of the specimen or cumbersome specimen preparations necessary nor have restrictions regarding the specific specimen geometry to be imposed. Furthermore, unlike in numerical simulation approaches, specimen variability can be accounted for by considering material-dependent parameters as uncertain and by using actual, specimen-specific measurement data.

The paper is organised as follows: Section 2 recalls the fundamentals of Bayesian inference and gives theoretical background on the utilised recursive filtering and smoothing methods. In Section 3, the experimental procedure is presented and harnessed to derive the subsequently applied state space definition. The Section is completed with insight into the adopted algorithm operation. In Section 4, the results obtained by the Bayesian approach are presented and discussed whereas Section 5 concludes the paper.

2 BAYESIAN APPROACH

The modelling of dynamic processes with imperfect or unknown information gives rise to numerous sources of uncertainty and variability that have to be accounted for [13–16]. These sources contribute to the system's state uncertainty, the modelling uncertainty and - in terms of prognosis - the future uncertainty. The state of a system is uncertain since it is determined indirectly via observations where uncertainty can be recognised in the measurement method itself as well as in the governing measuring parameters that are fixed, yet unknown. Furthermore, the model representing the dynamic process incorporates uncertainty as the true phenomenon under consideration can only be depicted adequately to a certain degree. This includes the mathematical expressions as well as the uncertainty in unknown fixed and variable model parameters. In addition, predictions about future states entail uncertainty associated with not controllable quantities influencing the states. All these uncertainties have to be *represented*, *quantified* and *propagated*.

The inverse problem of identifying unknown states given a set of observations is herein addressed in a probabilistic setting by a Bayesian approach that exhibits three main features:

(I) Such inverse problems are typically ill-posed as the states are often overfitted or underdetermined. By means of regularisation, additional assumptions on the states can be introduced to circumvent the issue. This approach corresponds to incorporating prior information in Bayesian inference, which is why many inverse problems become *well-posed* when formulated in a Bayesian fashion [10, 17].

(II) Defining a probabilistic state space model, all quantities of interest are modelled as random variables with corresponding probability distributions. The randomness expresses the *degree of belief* or *amount of information* about their true values and represents the uncertainty

associated with these unknown quantities.

(III) The objective in the context of solving an inverse problem ist not limited to *identifying* a particular set of states and parameters that optimally satisfies an arbitrary condition, like for example minimising the expected value of a loss function. Utilising a Bayesian approach, the unknown states are *inferred* from given observations, i.e. new available data is used to adjust the prior belief or knowledge about the states in a probabilistic manner, thereby allowing for systematic uncertainty quantification and uncertainty propagation [18].

2.1 Bayesian filtering and smoothing in parameter estimation

Let $\boldsymbol{x}_{0:T} = \{\boldsymbol{x}_0, \dots, \boldsymbol{x}_T\}$ and $\boldsymbol{y}_{1:T} = \{\boldsymbol{y}_1, \dots, \boldsymbol{y}_T\}$ denote a vector-valued time series of hidden states $\boldsymbol{x}_k \in \mathbb{R}^{d_x}$ and observed measurements $\boldsymbol{y}_k \in \mathbb{R}^{d_y}$ at time step k up to a last time step T, $\boldsymbol{\theta} \in \mathbb{R}^{d_\theta}$ a vector containing the unknown parameters and $p(\cdot)$ the probability distribution of a continuous random variable. In Bayesian inference the joint posterior distribution of the states and parameters given the measurements can then be computed via Bayes' rule as

$$p(\boldsymbol{x}_{0:T}, \boldsymbol{\theta} | \boldsymbol{y}_{1:T}) = \frac{p(\boldsymbol{y}_{1:T} | \boldsymbol{x}_{0:T}, \boldsymbol{\theta}) p(\boldsymbol{x}_{0:T} | \boldsymbol{\theta}) p(\boldsymbol{\theta})}{p(\boldsymbol{y}_{1:T})}. \tag{1}$$

Since discrete-time observations provide sequential data, it is more efficient and generally more convenient to only infer the current state and parameters on the basis of the preceding ones. Applying a recursive prediction and update scheme with due regard to the Markov property of states and the conditional independence of measurements and the thus ensuing implications for the choice of dynamic models [2] yields the desired effect and ensures a constant number of computations per time step. The predictive distribution of the state $\boldsymbol{x}_k$ at time step k given the measurements up to time step $k-1$ and the unknown parameters is given by the Chapman-Kolmogorov equation as

$$p(\boldsymbol{x}_k | \boldsymbol{y}_{1:k-1}, \boldsymbol{\theta}) = \int p(\boldsymbol{x}_k | \boldsymbol{x}_{k-1}, \boldsymbol{\theta}) p(\boldsymbol{x}_{k-1} | \boldsymbol{y}_{1:k-1}, \boldsymbol{\theta}) \mathrm{d}\boldsymbol{x}_{k-1}, \tag{2}$$

where $p(\boldsymbol{x}_k | \boldsymbol{x}_{k-1}, \boldsymbol{\theta})$ is the dynamic model. It characterises probabilistically the propagation of the states in time. The posterior distribution of the state $\boldsymbol{x}_k$ given the measurements up to time step k and the unknown parameters follows from Bayes' rule as

$$p(\boldsymbol{x}_k | \boldsymbol{y}_{1:k}, \boldsymbol{\theta}) = \frac{p(\boldsymbol{y}_k | \boldsymbol{x}_k, \boldsymbol{\theta}) p(\boldsymbol{x}_k | \boldsymbol{y}_{1:k-1}, \boldsymbol{\theta})}{p(\boldsymbol{y}_k | \boldsymbol{y}_{1:k-1}, \boldsymbol{\theta})}, \tag{3}$$

where $p(\boldsymbol{y}_k | \boldsymbol{x}_k, \boldsymbol{\theta})$ is the measurement model. The *prediction step* in Eq. (2) and *update step* in Eq. (3) together constitute the recursive *Bayesian filtering equations* [19] and allow for the inference of the states $\boldsymbol{x}_k$. In order to infer the unknown parameters $\boldsymbol{\theta}$, the filtering expressions have to be complemented by the marginalised joint posterior distribution of the parameters given the measurements:

$$p(\boldsymbol{\theta} | \boldsymbol{y}_{1:k}) = p(\boldsymbol{\theta} | \boldsymbol{y}_{1:k-1}) \int \frac{p(\boldsymbol{y}_k | \boldsymbol{x}_k, \boldsymbol{\theta}) p(\boldsymbol{x}_k | \boldsymbol{y}_{1:k-1}, \boldsymbol{\theta})}{p(\boldsymbol{y}_k | \boldsymbol{y}_{1:k-1})} \mathrm{d}\boldsymbol{x}_k. \tag{4}$$

Thereby, the inference on the fixed but unknown parameters is enhanced at every time step in the presence of new observations. Beyond incorporating new observations to update the current state and to predict future ones, to adjust preceding states might be beneficial given the context

as well. By conditioning previous states on *all* observations (including future observations) as in

$$p(\boldsymbol{x}_k|\boldsymbol{y}_{1:T},\boldsymbol{\theta}) = p(\boldsymbol{x}_k|\boldsymbol{y}_{1:k},\boldsymbol{\theta}) \int \frac{p(\boldsymbol{x}_{k+1}|\boldsymbol{x}_k,\boldsymbol{\theta})p(\boldsymbol{x}_{k+1}|\boldsymbol{y}_{1:T},\boldsymbol{\theta})}{p(\boldsymbol{x}_{k+1}|\boldsymbol{y}_{1:k},\boldsymbol{\theta})}\mathrm{d}\boldsymbol{x}_{k+1}, \tag{5}$$

the marginal posterior distribution of the state $\boldsymbol{x}_k$ given all observations up to time step T with $T > k$ can be obtained in a *smoothing step*. Finally, by formally modelling an observable dynamic process as probabilistic state space model of the following form

$$\begin{aligned} \boldsymbol{\theta} &\sim p(\boldsymbol{\theta}), \\ \boldsymbol{x}_0 &\sim p(\boldsymbol{x}_0|\boldsymbol{\theta}), \\ \boldsymbol{x}_k &\sim p(\boldsymbol{x}_k|\boldsymbol{x}_{k-1},\boldsymbol{\theta}), \\ \boldsymbol{y}_k &\sim p(\boldsymbol{y}_k|\boldsymbol{x}_k,\boldsymbol{\theta}), \end{aligned} \tag{6}$$

the issue of solving the inverse problem can be approached by Bayesian filtering and smoothing.

Closed form solutions for Eq. (2) to (5) generally exist only for a few classes of filtering and smoothing problems. For linear Gaussian state space models, optimal Bayesian solutions can be obtained by means of the Kalman filter [20] and Rauch-Tung-Striebel smoother [21]. In terms of finite state space models, grid-based methods can be utilised to provide an optimal solution [22,23]. However, a variety of approximate filtering and smoothing methods for nonlinear and infinite state space models exist, which encompass inter alia Gaussian filtering and smoothing methods [19], Monte Carlo Sampling approaches [23] and approximate grid-based methods [24]. The former can be considered as local approaches, the two latter as global approaches [25].

In the present paper, a combination of local and global approaches is utilised which is why further insight into these methods is given hereafter.

2.2 Unscented transform for filtering and smoothing

The *unscented Kalman filter* (UKF) [26–28] as well as the *unscented Rauch-Tung-Striebel smoother* (URTSS) [19] address the filtering and smoothing problem by utilising the unscented transform as a way of deterministic sampling [14] in a Gaussian framework. Considering two random variables $\boldsymbol{\xi}$ and $\boldsymbol{\upsilon}$ with a nonlinear model function $\boldsymbol{\upsilon} = g(\boldsymbol{\xi})$, an approximation to the joint distribution can be obtained by estimating the mean $\boldsymbol{\mu}_{\boldsymbol{\upsilon}}$ and covariance $\boldsymbol{\Sigma}_{\boldsymbol{\upsilon}\boldsymbol{\upsilon}}$ by means of a minimal set of weighted samples. These so called sigma points $\boldsymbol{\mathcal{X}}^i$ are chosen deterministically and propagated through the respective model to form new sigma points $\boldsymbol{\mathcal{Y}}^i = g(\boldsymbol{\mathcal{X}}^i)$ and compute mean and covariance:

$$\boldsymbol{\mu}_{\boldsymbol{\upsilon}} = \sum_i W^i \boldsymbol{\mathcal{Y}}^i, \tag{7}$$

$$\boldsymbol{\Sigma}_{\boldsymbol{\upsilon}\boldsymbol{\upsilon}} = \sum_i W^i (\boldsymbol{\mathcal{Y}}^i - \boldsymbol{\mu}_{\boldsymbol{\upsilon}})(\boldsymbol{\mathcal{Y}}^i - \boldsymbol{\mu}_{\boldsymbol{\upsilon}})^{\mathrm{T}}. \tag{8}$$

Assuming an a priori Gaussian state distribution as well as additive Gaussian noise in the dynamic and measurement models

$$\boldsymbol{x}_k = \boldsymbol{f}(\boldsymbol{x}_{k-1},\boldsymbol{\theta}) + \boldsymbol{q}_{k-1}, \tag{9}$$

$$\boldsymbol{y}_k = \boldsymbol{h}(\boldsymbol{x}_k,\boldsymbol{\theta}) + \boldsymbol{r}_k, \tag{10}$$

where $\boldsymbol{f}(\cdot)$ is the dynamic transition function, $\boldsymbol{h}(\cdot)$ is the measurement function, $\boldsymbol{q}_{k-1} \sim \mathcal{N}(0, \boldsymbol{Q}_{k-1})$ is the process noise and $\boldsymbol{r}_k \sim \mathcal{N}(0, \boldsymbol{R}_k)$ the noise of measurements, Gaussian approximations to the filtering distributions in Eq. (2) and (3) can be obtained as

$$\begin{aligned} p(\boldsymbol{x}_k|\boldsymbol{y}_{1:k-1}, \boldsymbol{\theta}) &\approx \mathcal{N}(\boldsymbol{x}_k|\boldsymbol{m}_k^-(\boldsymbol{\theta}), \boldsymbol{P}_k^-(\boldsymbol{\theta})), \\ p(\boldsymbol{x}_k|\boldsymbol{y}_{1:k}, \boldsymbol{\theta}) &\approx \mathcal{N}(\boldsymbol{x}_k|\boldsymbol{m}_k(\boldsymbol{\theta}), \boldsymbol{P}_k(\boldsymbol{\theta})) \end{aligned} \tag{11}$$

by utilising the UKF. In the *prediction step*, the mean $\boldsymbol{m}_k^-(\boldsymbol{\theta})$ and covariance $\boldsymbol{P}_k^-(\boldsymbol{\theta})$ which depend on $\boldsymbol{\theta}$ are computed by

- forming the sigma points

$$\boldsymbol{\mathcal{X}}_{k-1}^i(\boldsymbol{\theta}) = \begin{cases} \boldsymbol{m}_{k-1}(\boldsymbol{\theta}), & i = 0 \\ \boldsymbol{m}_{k-1}(\boldsymbol{\theta}) + \sqrt{d_x + \lambda}\sqrt{\boldsymbol{P}_{k-1}(\boldsymbol{\theta})}, & i = 1, \dots, d_x \\ \boldsymbol{m}_{k-1}(\boldsymbol{\theta}) - \sqrt{d_x + \lambda}\sqrt{\boldsymbol{P}_{k-1}(\boldsymbol{\theta})}, & i = d_x + 1, \dots, 2d_x, \end{cases} \tag{12}$$

- propagating the sigma points

$$\hat{\boldsymbol{\mathcal{X}}}_k^i(\boldsymbol{\theta}) = \boldsymbol{f}(\boldsymbol{\mathcal{X}}_{k-1}^i(\boldsymbol{\theta})), \quad i = 0, \dots, 2d_x, \tag{13}$$

- which yields

$$\begin{aligned} \boldsymbol{m}_k^-(\boldsymbol{\theta}) &= \sum_{i=0}^{2d_x} W^i \hat{\boldsymbol{\mathcal{X}}}_k^i(\boldsymbol{\theta}), \\ \boldsymbol{P}_k^-(\boldsymbol{\theta}) &= \sum_{i=0}^{2d_x} W^i \left(\hat{\boldsymbol{\mathcal{X}}}_k^i(\boldsymbol{\theta}) - \boldsymbol{m}_k^-(\boldsymbol{\theta})\right) \left(\hat{\boldsymbol{\mathcal{X}}}_k^i(\boldsymbol{\theta}) - \boldsymbol{m}_k^-(\boldsymbol{\theta})\right)^{\mathrm{T}} + \boldsymbol{Q}_{k-1}. \end{aligned} \tag{14}$$

In the *update step*, the mean $\boldsymbol{m}_k(\boldsymbol{\theta})$ and covariance $\boldsymbol{P}_k(\boldsymbol{\theta})$ are computed by

- forming the sigma points

$$\boldsymbol{\mathcal{X}}_k^{-i}(\boldsymbol{\theta}) = \begin{cases} \boldsymbol{m}_k^-(\boldsymbol{\theta}), & i = 0 \\ \boldsymbol{m}_k^-(\boldsymbol{\theta}) + \sqrt{d_x + \lambda}\sqrt{\boldsymbol{P}_k^-(\boldsymbol{\theta})}, & i = 1, \dots, d_x \\ \boldsymbol{m}_k^-(\boldsymbol{\theta}) - \sqrt{d_x + \lambda}\sqrt{\boldsymbol{P}_k^-(\boldsymbol{\theta})}, & i = d_x + 1, \dots, 2d_x, \end{cases} \tag{15}$$

- propagating the sigma points

$$\hat{\boldsymbol{\mathcal{Y}}}_k^i(\boldsymbol{\theta}) = \boldsymbol{h}(\boldsymbol{\mathcal{X}}_k^{-i}(\boldsymbol{\theta})), \quad i = 0, \dots, 2d_x, \tag{16}$$

- calculating

$$\begin{aligned} \boldsymbol{\mu}_k(\boldsymbol{\theta}) &= \sum_{i=0}^{2d_x} W^i \hat{\boldsymbol{\mathcal{Y}}}_k^i(\boldsymbol{\theta}), \\ \boldsymbol{S}_k(\boldsymbol{\theta}) &= \sum_{i=0}^{2d_x} W^i \left(\hat{\boldsymbol{\mathcal{Y}}}_k^i(\boldsymbol{\theta}) - \boldsymbol{\mu}_k(\boldsymbol{\theta})\right) \left(\hat{\boldsymbol{\mathcal{Y}}}_k^i(\boldsymbol{\theta}) - \boldsymbol{\mu}_k(\boldsymbol{\theta})\right)^{\mathrm{T}} + \boldsymbol{R}_k, \\ \boldsymbol{C}_k(\boldsymbol{\theta}) &= \sum_{i=0}^{2d_x} W^i \left(\hat{\boldsymbol{\mathcal{X}}}_k^{-i}(\boldsymbol{\theta}) - \boldsymbol{m}_k^-(\boldsymbol{\theta})\right) \left(\hat{\boldsymbol{\mathcal{Y}}}_k^i(\boldsymbol{\theta}) - \boldsymbol{\mu}_k(\boldsymbol{\theta})\right)^{\mathrm{T}}, \\ \boldsymbol{K}_k(\boldsymbol{\theta}) &= \boldsymbol{C}_k \boldsymbol{S}_k(\boldsymbol{\theta})^{-1}, \end{aligned} \tag{17}$$

- which yields

$$\begin{aligned}\boldsymbol{m}_k(\boldsymbol{\theta}) &= \boldsymbol{m}_k^-(\boldsymbol{\theta}) + \boldsymbol{K}_k(\boldsymbol{\theta})\left[\boldsymbol{y}_k(\boldsymbol{\theta}) - \boldsymbol{\mu}_k(\boldsymbol{\theta})\right],\\ \boldsymbol{P}_k(\boldsymbol{\theta}) &= \boldsymbol{P}_k^-(\boldsymbol{\theta}) - \boldsymbol{K}_k(\boldsymbol{\theta})\boldsymbol{S}_k(\boldsymbol{\theta})\boldsymbol{K}_k^{\mathrm{T}}(\boldsymbol{\theta}).\end{aligned} \tag{18}$$

The free parameter λ is a scaling quantity that should be set to $\lambda = 3 - d_x$ for Gaussian state variables on a heuristic bases [26]. The weights W^i can be computed as

$$W^i = \begin{cases} \dfrac{\lambda}{d_x + \lambda}, & i = 0\\ \dfrac{\lambda}{2(d_x + \lambda)}, & i = 1, \ldots, 2d_x. \end{cases} \tag{19}$$

Recalling the complementation of the Bayesian filtering distributions by the marginalised joint posterior distribution of the parameters given the measurements $p(\boldsymbol{\theta}|\boldsymbol{y}_{1:k})$ in Eq. (4), the estimation of the unknown parameters has to be addressed as well. The equation is rewritten [29] as

$$\begin{aligned} p(\boldsymbol{\theta}|\boldsymbol{y}_{1:k}) &= p(\boldsymbol{\theta}|\boldsymbol{y}_{1:k-1}) \int \frac{p(\boldsymbol{y}_k|\boldsymbol{x}_k, \boldsymbol{\theta}) p(\boldsymbol{x}_k|\boldsymbol{y}_{1:k-1}, \boldsymbol{\theta})}{p(\boldsymbol{y}_k|\boldsymbol{y}_{1:k-1})} \mathrm{d}\boldsymbol{x}_k\\ &\propto p(\boldsymbol{\theta}|\boldsymbol{y}_{1:k-1}) p(\boldsymbol{y}_k|\boldsymbol{y}_{1:k-1}, \boldsymbol{\theta}), \end{aligned} \tag{20}$$

whereas the second term is obtained as Gaussian approximation

$$p(\boldsymbol{y}_k|\boldsymbol{y}_{1:k-1}, \boldsymbol{\theta}) \approx \mathcal{N}(\boldsymbol{y}_k|\boldsymbol{\mu}_k(\boldsymbol{\theta}), \boldsymbol{S}_k(\boldsymbol{\theta})). \tag{21}$$

The corresponding mean $\boldsymbol{\mu}_k(\boldsymbol{\theta})$ and covariance $\boldsymbol{S}_k(\boldsymbol{\theta})$ are the results of the calculation in Eq. (17).

By means of the unscented Rauch-Tung-Striebel smoother (URTSS), a Gaussian approximations to the smoothing distribution in Eq. (5) can be obtained as

$$p(\boldsymbol{x}_k|\boldsymbol{y}_{1:T}, \boldsymbol{\theta}) \approx \mathcal{N}(\boldsymbol{x}_k|\boldsymbol{m}_k^{\mathrm{s}}(\boldsymbol{\theta}), \boldsymbol{P}_k^{\mathrm{s}}(\boldsymbol{\theta})). \tag{22}$$

In the *smoothing step*, the mean $\boldsymbol{m}_k^{\mathrm{s}}(\boldsymbol{\theta})$ and covariance $\boldsymbol{P}_k^{\mathrm{s}}(\boldsymbol{\theta})$ are computed by

- forming the sigma points

$$\boldsymbol{\mathcal{X}}_k^i(\boldsymbol{\theta}) = \begin{cases} \boldsymbol{m}_k(\boldsymbol{\theta}), & i = 0\\ \boldsymbol{m}_k(\boldsymbol{\theta}) + \sqrt{d_x + \lambda}\sqrt{\boldsymbol{P}_k(\boldsymbol{\theta})}, & i = 1, \ldots, d_x\\ \boldsymbol{m}_k(\boldsymbol{\theta}) - \sqrt{d_x + \lambda}\sqrt{\boldsymbol{P}_k(\boldsymbol{\theta})}, & i = d_x + 1, \ldots, 2d_x, \end{cases} \tag{23}$$

- propagating the sigma points

$$\hat{\boldsymbol{\mathcal{X}}}_{k+1}^i(\boldsymbol{\theta}) = \boldsymbol{f}(\boldsymbol{\mathcal{X}}_k^i(\boldsymbol{\theta})), \quad i = 0, \ldots, 2d_x, \tag{24}$$

- calculating

$$\begin{aligned} \boldsymbol{m}_{k+1}^-(\boldsymbol{\theta}) &= \sum_{i=0}^{2d_x} W^i \hat{\boldsymbol{\mathcal{X}}}_{k+1}^i(\boldsymbol{\theta}),\\ \boldsymbol{P}_{k+1}^-(\boldsymbol{\theta}) &= \sum_{i=0}^{2d_x} W^i \left(\hat{\boldsymbol{\mathcal{X}}}_{k+1}^i(\boldsymbol{\theta}) - \boldsymbol{m}_{k+1}^-(\boldsymbol{\theta})\right)\left(\hat{\boldsymbol{\mathcal{X}}}_{k+1}^i(\boldsymbol{\theta}) - \boldsymbol{m}_{k+1}^-(\boldsymbol{\theta})\right)^{\mathrm{T}} + \boldsymbol{Q}_k,\\ \boldsymbol{D}_{k+1}(\boldsymbol{\theta}) &= \sum_{i=0}^{2d_x} W^i \left(\hat{\boldsymbol{\mathcal{X}}}_k^i(\boldsymbol{\theta}) - \boldsymbol{m}_k(\boldsymbol{\theta})\right)\left(\hat{\boldsymbol{\mathcal{X}}}_{k+1}^i(\boldsymbol{\theta}) - \boldsymbol{m}_{k+1}^-(\boldsymbol{\theta})\right)^{\mathrm{T}}, \end{aligned} \tag{25}$$

- which yields

$$\begin{aligned}
\boldsymbol{G}_k(\boldsymbol{\theta}) &= \boldsymbol{D}_{k+1}(\boldsymbol{\theta}) \left[\boldsymbol{P}^-_{k+1}(\boldsymbol{\theta})\right]^{-1}, \\
\boldsymbol{m}^{\mathrm{s}}_k(\boldsymbol{\theta}) &= \boldsymbol{m}_k(\boldsymbol{\theta}) + \boldsymbol{G}_k(\boldsymbol{\theta}) \left[\boldsymbol{m}^{\mathrm{s}}_{k+1}(\boldsymbol{\theta}) - \boldsymbol{m}^-_{k+1}(\boldsymbol{\theta})\right], \\
\boldsymbol{P}^{\mathrm{s}}_k(\boldsymbol{\theta}) &= \boldsymbol{P}_k(\boldsymbol{\theta}) + \boldsymbol{G}_k(\boldsymbol{\theta}) \left[\boldsymbol{P}^{\mathrm{s}}_{k+1}(\boldsymbol{\theta}) - \boldsymbol{P}^-_{k+1}(\boldsymbol{\theta})\right] \boldsymbol{G}^{\mathrm{T}}_k(\boldsymbol{\theta}).
\end{aligned} \tag{26}$$

2.3 Approximate grid-based filtering

In *approximate grid-based filtering* [22,23], the continuous state space is decomposed into pre-defined cells and the filtering distributions are approximated by a weighted sum of δ functions. Discretising the state space into a finite number of states $\{\boldsymbol{x}^j : j = 1, \ldots, N_x\}$, the filtering solutions in Eq. (2) and (3) can be obtained as

$$\begin{aligned}
p(\boldsymbol{x}_k|\boldsymbol{y}_{1:k-1}, \boldsymbol{\theta}) &\approx \sum_{j=1}^{N_x} w^j_{k|k-1} \delta(\boldsymbol{x}_k - \boldsymbol{x}^j_k), \\
p(\boldsymbol{x}_k|\boldsymbol{y}_{1:k}, \boldsymbol{\theta}) &\approx \sum_{j=1}^{N_x} w^j_{k|k} \delta(\boldsymbol{x}_k - \boldsymbol{x}^j_k)
\end{aligned} \tag{27}$$

where the weights $w^j_{k|k-1}$ and $w^j_{k|k}$ represent the conditional probabilities of $\boldsymbol{x}^j$ given the measurements $\boldsymbol{y}_{1:k}$ respectively $\boldsymbol{y}_{1:k-1}$ and the parameters $\boldsymbol{\theta}$. They are computed as

$$w^j_{k|k-1} = \sum_{l=1}^{N_x} w^l_{k-1|k-1} p(\boldsymbol{x}^j_k|\boldsymbol{x}^l_{k-1}, \boldsymbol{\theta}), \tag{28}$$

$$w^j_{k|k} = \frac{w^j_{k|k-1} p(\boldsymbol{y}_k|\boldsymbol{x}^j_k, \boldsymbol{\theta})}{\sum_{l=1}^{N_x} w^l_{k|k-1} p(\boldsymbol{y}_k|\boldsymbol{x}^l_k, \boldsymbol{\theta})}, \tag{29}$$

where the initial weights are denoted as $w^j_{0|0} = p(\boldsymbol{x}^j_0|\boldsymbol{\theta}) / \sum_{l=1}^{N_x} p(\boldsymbol{x}^l_0|\boldsymbol{\theta})$. The approximations arise due to the fact that the probabilities are not integrated over the regions of the continuous state space but averaged for the discretised grid points $\boldsymbol{x}^j$. In order to obtain accurate approximations to the filtering distributions, the resolution of the grid has to be sufficiently fine which - in combination with a high dimension of the state - renders the approach computational burdensome.

3 PROBLEM STATEMENT

3.1 Experimental procedure

The fatigue testing is performed by subjecting Udimet 720Li superalloy specimens to cyclic uniaxial tensile stress within a convection oven at a temperature of $400\,^{\circ}\mathrm{C}$, see Figure 2. The quadratic bar specimens (side W) are pre-notched at a single corner to act as crack initiation point under a sinusoidal loading at $f = 10\,\mathrm{Hz}$ with the aim of overcoming non-continuum mechanics-governed and unstable crack growth [30]. A stable Mode-I crack propagation is then accomplished by a trapezoidal shape loading at $f = 0.25\,\mathrm{Hz}$. The crack surface is assumed to evolve in a quarter-circular shape which renders the equidistant length $r(\varphi)$ from pre-notched corner to crack front the single quantity a characterising the crack size. This simplification is reasonable as long as crack tunnelling can be ruled out [31].

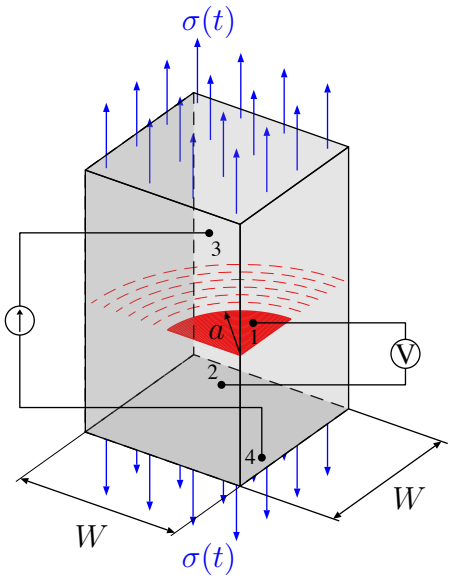

Figure 2: Experimental setup: Applied stress, geometries, crack propagation orientation as well as electrode and probe positioning

The crack size a can indirectly be measured conveniently by means of the DCPD method. Therefore, a direct current is supplied by electrodes near the lower and upper ends of the specimen (3 and 4 in Figure 2). Subsequently, the potential drop U is determined by measuring the potential difference between the respective crack surfaces via probes that are spot-welded in close proximity to the notch (1 and 2 in Figure 2). With increasing crack size a the obtained potential drop U scales accordingly, yielding time-dependent or more conveniently cycle-dependent values U_k at specific cycles N_k. With only roughly pre-defined probe positions, neither symmetry nor accuracy can be assumed, rendering the relationship between the cycle-dependent crack size a_k and potential drop U_k indeed quantifiable, however unknown. The relation can then be depicted as

$$U_k = c(a_k; \boldsymbol{b}) + \varepsilon_k \tag{30}$$

where c is an arbitrary function depending on the vector of unknown parameters $\boldsymbol{b}$ representing the calibration curve and ε_k is the error term for the particular observation at time step k.

For the purpose of assessing the proposed Bayesian model calibration and parameter estimation, reference damage propagation data have to be obtained. This is done by performing an additional experimental calibration by investigating the crack front of each specimen subsequent to the fatigue testing. Therefore, the specimens are cut in the respective crack propagation cross section where the fracture plane A_{fp} can be measured and utilised to average the crack sizes a_0 at the beginning and a_{end} at the end of the crack propagation as

$$a = \sqrt{\frac{4A_{\mathrm{fp}}}{\pi}}. \tag{31}$$

With the assumption of c being linear [6,32], the 3-tuples (N_0, U_0, a_0) and$(N_{\mathrm{end}}, U_{\mathrm{end}}, a_{\mathrm{end}})$ can be employed to determine $\boldsymbol{b}$ and subsequently interpolate a_k. The reference data are hereafter denoted as actual or true parameter and crack size values. The obtained data consists of six sample trajectories $\{U_k : k = 1, \ldots, n_{\mathrm{ms}}\}$ for specimens #1 to #6 (each subjected to various stress ranges and stress ratios) with 26 to 41 total measurements n_{ms}.

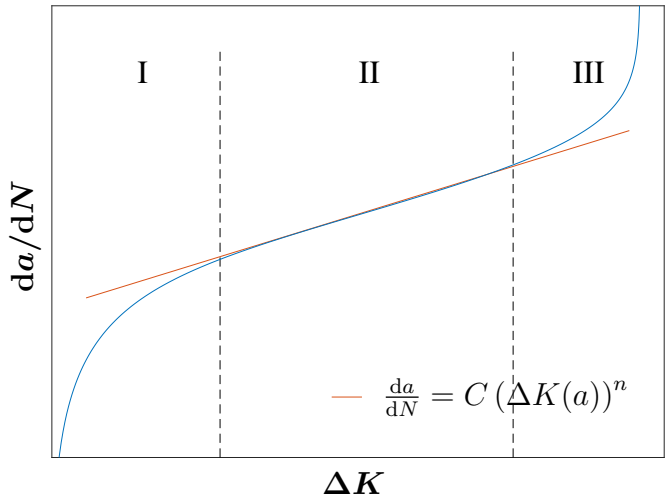

Figure 3: Schematic fatigue crack growth (logarithmic scales)

3.2 State space definition

Recalling the general form of the probabilistic SSM for observable dynamic processes in Eq. (6), different quantities have to be defined probabilistically in order to allow for the application of Bayesian filtering and smoothing. This definition encompasses the modelling of dynamic and measurement processes as well as prior information on the unknown states and parameters and is carried out hereafter for the corner crack fatigue testing presented in the preceding section.

When considering crack growth under fatigue loading, the damage evolution is generally characterised by three stages: (I) crack initiation, (II) stable crack growth, (III) instable crack growth and failure. It can be visualised by plotting the crack growth rate $\mathrm{d}a/\mathrm{d}N$ over the stress intensity factor (SIF) range ΔK as shown in Figure 3. The former describes the crack size increment per cycle. The latter depicts the range of stress intensity at the crack front tip which is dependent on the applied stress range $\Delta\sigma = \sigma_{\max} - \sigma_{\min}$ as well as the specific specimen geometry. A widely used formula utilised to model sub-critical, stable stage II crack growth is given by the Paris-Erdogan law [33,34]

$$\frac{\mathrm{d}a}{\mathrm{d}N} = C(\Delta K(a))^n, \tag{32}$$

where C and n are material-dependent scaling constants. The SIF range ΔK can be calculated for corner crack specimens [30] as

$$\Delta K(a) = \Delta\sigma g(a)\sqrt{\pi a}, \tag{33}$$

$$g(a) = M_{\mathrm{G}}(a)M_{\mathrm{B}}(a)M_{\mathrm{S}}(a)\frac{2}{\pi}, \tag{34}$$

where $g(a)$ is a crack-geometric correction factor that can be derived numerically for different specimen geometries and crack shapes and is given by [35]. The precise expressions for the individual shape functions $M_{\mathrm{G}}(a)$, $M_{\mathrm{B}}(a)$ and $M_{\mathrm{S}}(a)$ are omitted for the sake of clarity. Since only the stress range $\Delta\sigma$ is utilised in Eq. (32), mean stress effects are not taken into account [36]. In order to circumvent this problem, Paris' law can be improved by Walker's law [37], which is one among other modifications, e.g. [38–40]). It reads

$$\frac{\mathrm{d}a}{\mathrm{d}N} = C\left(\frac{\Delta K(a)}{(1-R_\sigma)^{1-\kappa}}\right)^n, \tag{35}$$

where $R_\sigma = \sigma_{\min}/\sigma_{\max}$ is the stress ratio and κ is an empirical constant weighing the influence of the mean stress on the crack growth rate (typically around 0.5 for metals). Where the aforementioned models fail to catch the sigmoidal shape of the crack growth rate plotted over the SIF range as depicted in Figure 3, a modification according to Forman/Mettu [41] allows for stage I and stage III crack growth depiction as well. It is given by

$$\frac{\mathrm{d}a}{\mathrm{d}N} = C \cdot F \cdot \Delta K(a)^n \frac{\left(1 - \frac{\Delta K_{\mathrm{th}}}{\Delta K(a)}\right)^p}{\left(1 - \frac{1}{1-R_\sigma}\frac{\Delta K(a)}{K_{\mathrm{c}}}\right)^q}, \tag{36}$$

where F is a crack velocity factor, ΔK_{th} is the threshold of SIF range for crack propagation, K_{c} is the fracture toughness and p, q are empirical constants [42]. In order to allow for a highly accurate representation of the crack propagation process of the available pre-notched specimens, a simplified and further modified Paris' law is obtained by setting $F = 1, q = 1, p = n$ [42] and introducing an additional exponent $m = 10$:

$$\frac{\mathrm{d}a}{\mathrm{d}N} = C \cdot \Delta K(a)^n \frac{\left(1 - \left(\frac{\Delta K_{\mathrm{th}}}{\Delta K(a)}\right)^m\right)^n}{1 - \frac{1}{1-R_\sigma}\frac{\Delta K(a)}{K_{\mathrm{c}}}}. \tag{37}$$

The rationale behind this approach is the following: In [2] where the model calibration was accomplished by means of Walker's law with fixed dynamic model parameters, the contribution of an appropriately represented test-initiation phase with a suitable dynamic model to the accuracy improvement was not investigated. By modifying the Forman/Mettu equation to a degree where an almost exact compliance with the reference data is feasible depending on the material-dependent parameters, the performance of the two dynamic models can be compared.

Both Walker's law in Eq. (35) and the Forman/Mettu equation in Eq. (36) are first order ordinary differential equations that can be numerically approximated for sufficiently small $\Delta N = N_k - N_{k-1}$ using finite differences and be rewritten as recurrence relation, yielding

$$a_k = a_{k-1} + \left.\frac{\mathrm{d}a}{\mathrm{d}N}\right|_{a=a_{k-1}} \Delta N \tag{38}$$

at time step k. Both equations are used to define the dynamic model and discussed later on: Where the Forman/Mettu equation allows a more precise depiction of the damage evolution, Walker's law comprises fewer unknown parameters.

As emphasised in Section 3.1, the relation between the measured potential drop and the crack size is assumed to be linear for corner crack specimens [6,32], yielding

$$U_k = b_1 a_k + b_2 + \varepsilon_k, \tag{39}$$

where b_1, b_2 are unknown and $\{\varepsilon_k, k = 1, \ldots, n_{\mathrm{ms}}\}$ has to be accounted for stochastically. If the assumption of linearity does not hold, for example in the case of specimens with a different crack geometry or more complex crack front shapes, the approach can be extended by using other forms, e.g. polynomial functions.

Let $x_k \in \mathbb{R}$ denote the crack size a_k, $y_k \in \mathbb{R}$ the potential drop measurement U_k at time step k and the vector $\boldsymbol{\theta} \in \mathbb{R}^{d_\theta}$ the collection of unknown parameters C, n, b_1, b_2 with $d_\theta = 4$ respectively $C, n, b_1, b_2, \Delta K_{\mathrm{th}}$ with $d_\theta = 5$. In order to account for existent uncertainties and variabilities as mentioned in Section 2, the hidden states $x_{0:n_{\mathrm{ms}}}$, the measurements $y_{1:n_{\mathrm{ms}}}$ and

the unknown parameters $\boldsymbol{\theta}$ are viewed as random variables that are assigned probability distributions, thereby expressing the degree of information concerning their realisations and the incorporated uncertainty. The initial state x_0 is supposed to be normally distributed with mean μ_0 and variance σ_0^2, since the process of notching the specimens is manageable to a certain degree. Since the threshold SIF range ΔK_{th} is dependent on the crack size as given in Eq. (33), the prior belief on θ_5 can be obtained by means of $x_0 \sim \mathcal{N}(\mu_0, \sigma_0^2)$. The remaining unknown parameters are initially assumed to be mutually independent random variables uniformly distributed on $[\underline{\theta}_1, \bar{\theta}_1] \times \ldots \times [\underline{\theta}_4, \bar{\theta}_4]$ because no prior information other then approximate boundaries are available. By further assuming constant additive Gaussian process noise $q \sim \mathcal{N}(0, Q)$ and Gaussian noise of measurements $r \sim \mathcal{N}(0, R)$ within the dynamic models and measurement model, the probabilistic state space model can then be defined as

$$x_k = f^{(\{I,II\})}(x_{k-1}, \boldsymbol{\theta}) + q, \tag{40}$$

$$y_k = h(x_k, \boldsymbol{\theta}) + r, \tag{41}$$

where the dynamic and measurement functions are

$$f^{(I)}(x_{k-1}, \boldsymbol{\theta}) = x_{k-1} + \theta_1 \left(\frac{\Delta K(x_{k-1})}{(1-R_\sigma)^{1-\kappa}} \right)^{\theta_2} \Delta N, \tag{42}$$

$$f^{(II)}(x_{k-1}, \boldsymbol{\theta}) = x_{k-1} + \theta_1 \Delta K(x_{k-1})^{\theta_2} \frac{\left(1 - \left(\frac{\theta_5}{\Delta K(x_{k-1})}\right)^m\right)^{\theta_2}}{1 - \frac{1}{1-R_\sigma}\frac{\Delta K(x_{k-1})}{K_{\mathrm{c}}}} \Delta N, \tag{43}$$

$$h(x_k, \boldsymbol{\theta}) = \theta_3 x_k + \theta_4. \tag{44}$$

3.3 Algorithm operation

With the unscented Kalman filter and the unscented Rauch-Tung-Striebel smoother as recursive approximations to the Bayesian inference in Section 2 and the ensuing definition of the probabilistic state space model in Section 3, the objective of finding a solution to the inverse problem of crack size estimation, model calibration and parameter estimation by means of potential drop measurements can be addressed as of yet only formally. Recalling the prediction, update and smoothing steps, the dependency of the state x_k on the unknown parameters $\boldsymbol{\theta}$ has to be propagated through every time step k resulting in nested functions that become ever more complex with each additional iteration. Therefore, a hybrid of local and global approaches in the form of the UKF/URTSS and approximate grid-based methods as depicted in Algorithm 1 is proposed. Similar methods have been used for example in [43–45] where particle filters instead of Gaussian filters are utilised in differing frameworks to compute the nodes in randomly or fixedly created grids in the parameter space, however with significant higher computational efforts.

As conceptually shown in Section 2.3 for the state space, the parameter space is now discretised into a finite number of cells $\{\boldsymbol{\theta}^j : j = 1, \ldots, N_\theta\}$, leading to recast Eq. (20) as

$$p(\boldsymbol{\theta}|y_{1:k}) \approx \sum_{j=1}^{N_\theta} w_{\boldsymbol{\theta}}^{k,j} \delta(\boldsymbol{\theta} - \boldsymbol{\theta}^j), \tag{45}$$

where the weights $w_{\boldsymbol{\theta}}^{k,j}$ can be computed by

$$w_{\boldsymbol{\theta}}^{k,j} \approx \frac{w_{\boldsymbol{\theta}}^{k-1,j} p(y_k|y_{1:k-1}, \boldsymbol{\theta}^j)}{\sum_{l=1}^{N_\theta} w_{\boldsymbol{\theta}}^{k-1,l} p(y_k|y_{1:k-1}, \boldsymbol{\theta}^l)}, \tag{46}$$

Algorithm 1 State and parameter estimation

set $x_0 \sim \mathcal{N}(\mu_0, \sigma_0^2)$
generate initial grid $\boldsymbol{\theta}^j$ and weights $w_{\boldsymbol{\theta}}^{0,j}$ for $\boldsymbol{\theta} \sim p(\boldsymbol{\theta})$
set $f(x_{k-1}, \boldsymbol{\theta})$
set $h(x_k, \boldsymbol{\theta})$
for $k = 1 : n_{\mathrm{ms}}$ **do**
    for $j = 1 : N_\theta$ **do** ▷ UKF steps
        compute $p(x_k|y_{1:k-1}, \boldsymbol{\theta}^j)$
        compute $p(x_k|y_{1:k}, \boldsymbol{\theta}^j)$
        compute $p(y_k|y_{1:k-1}, \boldsymbol{\theta}^j)$
        compute $w_{\boldsymbol{\theta}}^{k,j}$ by updating $w_{\boldsymbol{\theta}}^{k-1,j}$ ▷ Grid-based update
    end for
    compute $p(\boldsymbol{\theta}|y_{1:k})$
    ▷ MAP estimates
    evaluate $\hat{\boldsymbol{\theta}}^{\mathrm{MAP}}$
    set $\hat{x}_k = m_k^{j^*}$
    for $\alpha = 1 : d_\theta$ **do**
        compute $p(\theta_\alpha|y_{1:k})$ ▷ Marginalised posterior distributions
    end for
    compute $p(x_k|y_{1:k})$
    ▷ MMSE estimates
    evaluate $\hat{\boldsymbol{\theta}}^{\mathrm{MMSE}}$
    evaluate $\hat{x}_k^{\mathrm{MMSE}}$
end for
for $k = n_{\mathrm{ms}} - 1 : 1$ **do**
    compute $p(x_k|y_{1:T}, \hat{\boldsymbol{\theta}}^{\mathrm{MAP}})$ ▷ URTSS steps
    compute $p(x_k|y_{1:T}, \hat{\boldsymbol{\theta}}^{\mathrm{MMSE}})$
    ▷ Smoothing estimates
    evaluate $\hat{x}_k^{\mathrm{s,MAP}}$
    evaluate $\hat{x}_k^{\mathrm{s,MMSE}}$
end for

with the initial weights denoted as $w_{\boldsymbol{\theta}}^{0,j} = p(\boldsymbol{\theta}^j) / \sum_l^{N_\theta} p(\boldsymbol{\theta}^l)$. The recursive Bayesian filtering and smoothing expressions in Eq. (2), (3) and (5) then become

$$p(x_k|y_{1:k-1}, \boldsymbol{\theta}^j) = \int p(x_k|x_{k-1}, \boldsymbol{\theta}^j) p(x_{k-1}|y_{1:k-1}, \boldsymbol{\theta}^j) \mathrm{d}x_{k-1} \tag{47}$$

$$p(x_k|y_{1:k}, \boldsymbol{\theta}^j) = \frac{p(y_k|x_k, \boldsymbol{\theta}^j) p(x_k|y_{1:k-1}, \boldsymbol{\theta}^j)}{p(y_k|y_{1:k-1}, \boldsymbol{\theta}^j)}, \tag{48}$$

$$p(x_k|y_{1:T}, \boldsymbol{\theta}^j) = p(x_k|y_{1:k}, \boldsymbol{\theta}^j) \int \frac{p(x_{k+1}|x_k, \boldsymbol{\theta}^j) p(x_{k+1}|y_{1:T}, \boldsymbol{\theta}^j)}{p(x_{k+1}|y_{1:k}, \boldsymbol{\theta}^j)} \mathrm{d}x_{k+1}, \tag{49}$$

and have to be evaluated N_θ times for each $\boldsymbol{\theta}^j$ per time step.

In order to assess the performance of the Bayesian approach, different point estimates are obtained. With the proposed approach, the posterior knowledge inferred from the measurements and the prior information can be depicted in a more extensive manner, including variances and higher order moments. However, within the scope of this paper only point estimates are

considered. A natural choice is to maximise the posterior distribution of the parameters given the measurements to determine the parameter set with the highest probability as

$$\hat{\boldsymbol{\theta}}^{\mathrm{MAP}} = \arg\max_{\boldsymbol{\theta}} p(\boldsymbol{\theta}|y_{1:k}), \tag{50}$$

where $\hat{\boldsymbol{\theta}}^{\mathrm{MAP}} = \boldsymbol{\theta}^{j^*}$ is the maximum a posteriori (MAP) estimate of the parameters and j^* the corresponding index of the discretisation. The associated MAP estimate of the crack size can then by identified as

$$\hat{x}_k^{\mathrm{MAP}} = m_k^{j^*}. \tag{51}$$

Another obvious point estimate can be found in the minimum mean square error (MMSE) estimate of the marginal conditional posterior distributions,

$$\hat{\theta}_\alpha^{\mathrm{MMSE}} = \int \theta_\alpha p(\theta_\alpha|y_{1:k})\mathrm{d}\theta_\alpha. \tag{52}$$

The marginal conditional posterior distribution of the parameter given the measurements $p(\theta_\alpha|y_{1:k})$ can be obtained by summing over the respective other parameters in Eq. (45) for $\alpha = 1, \ldots, d_\theta$, i.e.

$$\begin{aligned}
p(\theta_1|y_{1:k}) &\approx \sum_{i=1}^{N_{\theta_1}} w_{\theta_1}^{k,i}\delta(\theta_1 - \theta_1^i), \quad w_{\theta_1}^{k,i} = \sum_{l=1}^{N_\theta/N_{\theta_1}} w_{\boldsymbol{\theta}}^{k,(l-1)N_{\theta_1}+i}, \\
p(\theta_2|y_{1:k}) &\approx \sum_{i=1}^{N_{\theta_2}} w_{\theta_2}^{k,i}\delta(\theta_2 - \theta_2^i), \quad w_{\theta_2}^{k,i} = \sum_{l=1}^{N_\theta/(N_{\theta_1}N_{\theta_2})} \sum_{j=1}^{N_{\theta_1}} w_{\boldsymbol{\theta}}^{k,j+(l-1)N_{\theta_1}N_{\theta_2}+(i-1)N_{\theta_1}}, \\
p(\theta_3|y_{1:k}) &\approx \sum_{i=1}^{N_{\theta_3}} w_{\theta_3}^{k,i}\delta(\theta_3 - \theta_3^i), \quad w_{\theta_3}^{k,i} = \sum_{l=1}^{N_\theta/(N_{\theta_1}N_{\theta_2}N_{\theta_3})} \sum_{j=1}^{N_{\theta_1}N_{\theta_2}} w_{\boldsymbol{\theta}}^{k,j+(l-1)N_{\theta_1}N_{\theta_2}N_{\theta_3}+(i-1)N_{\theta_1}N_{\theta_2}}, \\
&\vdots \qquad\qquad\qquad\qquad\qquad\quad \vdots \\
p(\theta_\alpha|y_{1:k}) &\approx \sum_{i=1}^{N_{\theta_\alpha}} w_{\theta_\alpha}^{k,i}\delta(\theta_\alpha - \theta_\alpha^i), \quad w_{\theta_\alpha}^{k,i} = \sum_{l=1}^{N_\theta/N_l} \sum_{j=1}^{N_j} w_{\boldsymbol{\theta}}^{k,j+(l-1)N_l+(i-1)N_j},
\end{aligned} \tag{53}$$

where

$$N_l = \prod_{\beta=1}^{\alpha} N_{\theta_\beta}, \qquad\qquad N_j = \prod_{\beta=1}^{\alpha-1} N_{\theta_\beta}.$$

The MMSE estimate of the parameters $\hat{\boldsymbol{\theta}}^{\mathrm{MMSE}}$ can then be computed by averaging over the weights for each of the d_θ parameters:

$$\hat{\theta}_\alpha^{\mathrm{MMSE}} \approx \sum_{i=1}^{N_{\theta_\alpha}} w_{\theta_\alpha}^{k,i}\theta_\alpha^i. \tag{54}$$

The marginalised conditional posterior distribution of the state given the measurements can be derived by integrating out the unknown parameters in Eq. (3) which - in terms of the discretised

parameter space - means summing over the product of the conditional posterior distribution of the state and the posterior distribution of the parameters:

$$p(x_k|y_{1:k}) = \int p(x_k|y_{1:k}, \boldsymbol{\theta}) p(\boldsymbol{\theta}|y_{1:k}) \mathrm{d}\boldsymbol{\theta}, \tag{55}$$

$$p(x_k|y_{1:k}) \approx \sum_{j=1}^{N_\theta} p(x_k|y_{1:k}, \boldsymbol{\theta}^j) w_{\boldsymbol{\theta}}^{k,j}. \tag{56}$$

By discretising the state space into a finite number of states $\{x^i : i = 1, \ldots, N_x\}$, the discrete approximation to Eq. (56) reads

$$p(x_k|y_{1:k}) \approx \sum_{i=1}^{N_x} w_x^{k,i} \delta(x_k - x_k^i), \qquad w_x^{k,i} = \frac{p(x_k^i|y_{1:k})}{\sum_{l=1}^{N_x} p(x_k^l|y_{1:k})}. \tag{57}$$

It can be utilised to compute the marginalised conditional posterior MMSE of the state analogously to Eq.(52) as

$$\hat{x}_k^{\mathrm{MMSE}} = \int x_k p(x_k|y_{1:k}) \mathrm{d}x_k,$$

$$\hat{x}_k^{\mathrm{MMSE}} \approx \sum_{i=1}^{N_x} w_x^{k,i} x_k^i. \tag{58}$$

4 RESULTS AND DISCUSSION

To begin with, the model calibration of the DCPD method is addressed, i.e. the estimation of the parameters $\{\theta_\alpha, \alpha = 3, 4\}$. In Figure 4, the normalised estimates of the measurement model parameters are plotted over the normalised cycles as to allow an accurate comparison for both dynamic model functions $f^{(\{I,II\})}(x_k, \boldsymbol{\theta})$ for all specimens of the test series. This direct comparison is possible since the actual parameter values are available due to the experimental calibration mentioned in Section 3.1. In addition to the MMSE and MAP estimates $\hat{\theta}_\alpha^{\mathrm{MMSE}}$ and $\hat{\theta}_\alpha^{\mathrm{MAP}}$, the ratio of relative deviation of the MMSE estimates and true parameter values of both dynamic models $|\hat{\theta}_\alpha^{\mathrm{MMSE}(\{I,II\})}/\theta_\alpha^{\mathrm{true}} - 1|$ is depicted for several intervals by means of stacked bars in corresponding colors (blue for dynamic model I, red for II). Initially assigned a uniform distribution at $N_0 = 0$, both parameter estimates vary noticeably at the beginning for both cases in Figure 4 (a) and (b). Where the MAP estimates remain almost constant for the first half of the cycles, the MMSE estimates diverge from their initial values towards the MAP estimates. In the latter half both parameter estimates approach in conjunction the actual underlying parameter values, albeit, not exhibiting convergence in the sense of an asymptotic behaviour. As pointed out in [2], different reasons can account for this shortcoming which encompass the variability of the material-dependent constants of the respective dynamic model and the possible inability of the dynamic model to cover specific physical behaviour. However, by introducing the dynamic model parameters θ_1 and θ_2 as additional random variables that are updated from step to step and therefore adjustable to the true underlying parameters instead of assigning them constant values, the asymptotic behaviour of the measurement model parameter estimates is not improved. This can partially be explained by the additional uncertainty incorporated into the SSM without compensation by more observations, i.e. a higher measuring rate. Likewise, the introduction

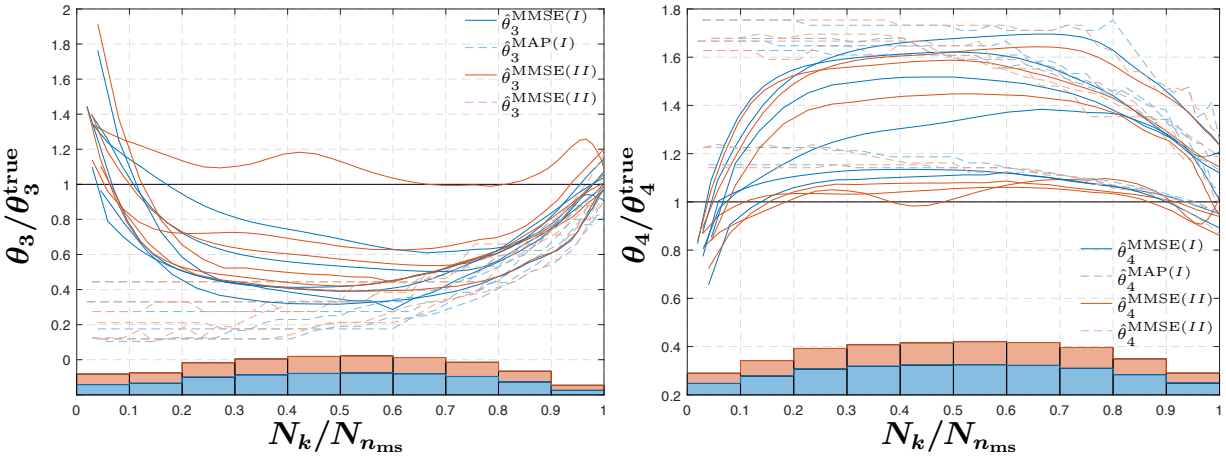

Figure 4: Model calibration: Normalised parameter estimates for θ_3 and θ_4 over normalised cycles N for dynamic models I (blue) and II (red) for all specimens as well as ratio of relative deviation of MMSE estimates and true parameter values (stacked bars in relative scale in corresponding colors).

of a further dynamic model that better accounts for the underlying physics yields no improved convergence since yet another parameter θ_5 is required to be modelled as random variable. An additional explanation stems from the inverse problem formulation itself: Considering the exponential crack growth characterised through the dynamic models, the inverse problem is not well-posed for the majority of the cycles where the crack growth is almost linear over time, yielding not a unique solution but various. This implies that the inference results improve the further the crack propagates and the more exponential the crack growth over cycles becomes. Beyond the question of asymptotic behaviour, it is apparent that the MMSE estimates reveal a higher accuracy than the corresponding MAP estimates. Furthermore, the aforementioned relative error bars show lower deviations of the MMSE estimates and true parameter values in the case of dynamic model II over I which is purchased by higher computational complexity.

The actual fatigue crack growth rate (reference data) is plotted over the stress intensity factor range for all specimens in Figure 5 in logarithmic scales. As elaborated on in Section 3.2, the two stages of test initiation and stable crack growth can be identified easily in Figure 5 (a). It is however apparent, that there are individual outliers especially in the initiation stage as well as deviations from the power growth behaviour in the stage of stable crack growth. In Figure 5 (b), the same plot is displayed in conjunction with both utilised dynamic models, the modified Paris' laws from Walker in Eq. (35) (solid lines) and from Forman/Mettu in Eq. (37) (dashed lines) where the MMSE estimates obtained at time step $k = n_{\text{ms}}$ are utilised as realisations of the parameters. Naturally, Walker's law allows only for the depiction of stable crack growth where the modified Paris' law by Forman/Mettu is able to cover the test-initiation phase of the entire crack propagation process as well. Nonetheless, the graphs of both dynamic models coincide for the phase of stable crack growth almost exactly, meaning the estimates for θ_1 and θ_2 do so as well. The MMSE parameter estimates $\hat{\theta}_1^{\text{MMSE}}$ and $\hat{\theta}_2^{\text{MMSE}}$ used in both dynamic models allow for a very good coverage of the crack growth rate in stage II of specimens $\#1$, $\#2$ and $\#6$ whereas only the latter measurements of specimens $\#3$ and $\#4$ show good compliance. Additionally, the test initiation phase can well be displayed using the obtained MMSE parameter

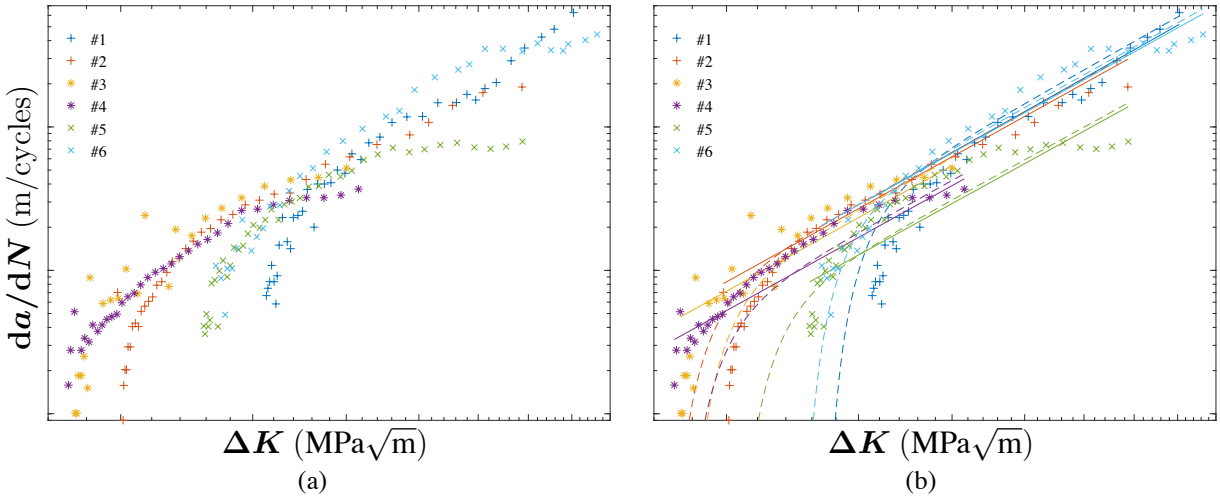

Figure 5: Fatigue crack growth rate over SIF range for all six specimens in logarithmic scales (axis tick labels omitted by virtue of proprietary information): (a) without, (b) with corresponding dynamic models I (solid lines) and II (dashed lines).

estimates $\hat{\theta}_{\alpha}^{\mathrm{MMSE}(II)}$ for $\alpha = 1, 2, 5$ in the Forman/Mettu modification for specimens $\#3$, $\#4$ and $\#6$. With the estimates θ_1 and θ_2 almost coinciding, the main difference in the usage of both dynamic models can therefore be ascribed to covering test-initiation as expected.

In Figure 6, the normalised filtering (a) and smoothing (b) estimates of the crack size are plotted over the normalised cycles for dynamic model functions $f^{\{(I,II)\}}(x_k, \boldsymbol{\theta})$ for all six specimens. Again, the ratio of relative deviation of the MMSE estimates and true crack size of both dynamic models $|\hat{x}_k^{\mathrm{MMSE}(\{I,II\})}/x_k^{\mathrm{true}} - 1|$ and $|\hat{x}_k^{\mathrm{s,MMSE}(\{I,II\})}/x_k^{\mathrm{true}} - 1|$ is depicted for several intervals by means of stacked bars in corresponding colors (blue for dynamic model I, red for II). The distinction of the plots in Figure 6 (a) and (b) lies in the conditioning of the respective estimates: In (a), the crack size estimates $\hat{x}_k$ are conditioned on all measurements $y_{1:k}$ up to time step k. The estimates $\hat{x}_k$ therefore correspond to the information available at time step k throughout the testing. In (b), the crack size estimates $\hat{x}_k^{\mathrm{s}}$ are - at every time step k - conditioned on all measurements $y_{1:n_{\mathrm{ms}}}$ which represents a refinement of the previously inferred estimates subsequent to the test. Both plots emphasise the better results that can be obtained via the MMSE estimates in comparison with the MAP estimates. Furthermore, the estimates inferred by utilisation of dynamic model II display a better performance in qualitative (graphs) as in quantitative (deviation error bars) regard. Considering that the absolute deviations decrease over the cycles when the relative errors remain constant (due to the normalising with the true crack size x_k^{true} at the specific cycle k) and taking into account that the crack size estimates approach the true values at the end of the tests, accurate results by the Bayesian approach can be observed. Considering the filtering estimates in Figure 6 (a), it is however apparent that, as with the estimates of θ_3 and θ_4 in Figure 4, no convergence is discernible. As mentioned before, this shortcoming might be circumvented by a higher measuring rate in general and especially a higher weighting of and increased emphasis on the latter part of the stable crack growth stage. In doing so, the computational expense must be kept in mind to allow for a compromise between accuracy (number of measurements, number of grid points) and timely availability in real-time crack size assessment.

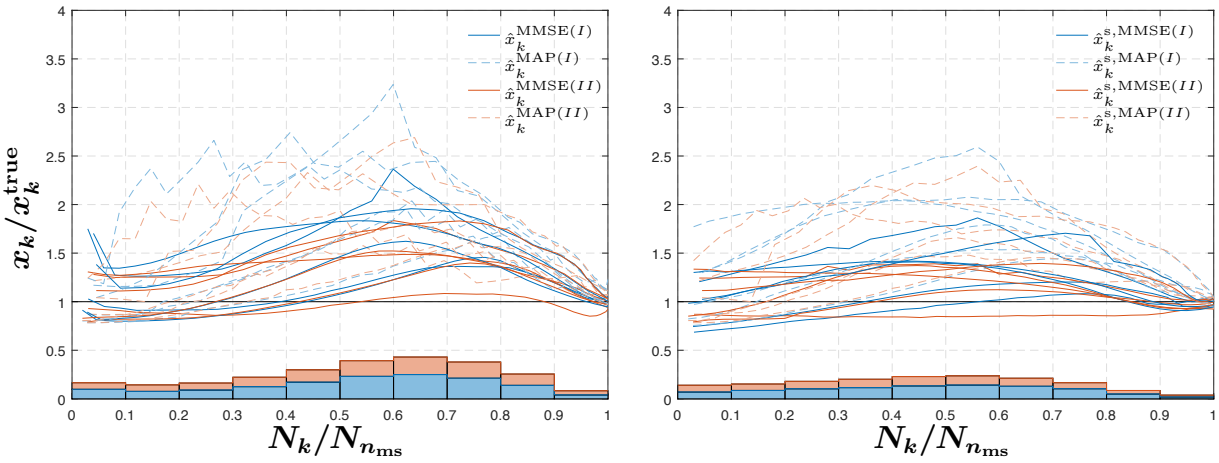

(a) Filtering estimates $\hat{x}_k^{\mathrm{MMSE}}$ and $\hat{x}_k^{\mathrm{MAP}}$

(b) Smoothing estimates $\hat{x}_k^{\mathrm{s,MMSE}}$ and $\hat{x}_k^{\mathrm{s,MAP}}$

Figure 6: Normalised crack size estimates over normalised cycles N_k for dynamic models I (blue) and II (red) for all specimens as well as ratio of absolute relative deviation of MMSE estimates $\hat{x}_k^{\mathrm{MMSE}}$, $\hat{x}_k^{\mathrm{s,MMSE}}$ from true crack size (stacked bars in relative scale in corresponding colors).

5 CONCLUSION

A Bayesian approach to the challenge of model calibration in DCPD measuring in conjunction with unknown material-dependent parameter estimation has been presented. Fatigue-tested corner crack specimens are monitored by means of the DCPD method without further knowledge of the calibration curve and the parameters governing the utilised physical models. The obtained potential drop measurements are then used to infer the unknown quantities of crack size, calibration curve and dynamic model parameters and compared with reference data.

1. The proposed methodology is found to provide accurate estimates for both model calibration and parameter estimation while allowing for an accurate crack size growth monitoring, even though no clear convergence of parameter and crack size estimates but only the approach of the respective true underlying values is observable.

2. The utilisation of the modified Forman/Mettu law allows for visibly better estimates in comparison with Walker's law, implying that the test-initiation phase is to be depicted by the dynamic model as precise as possible. However, this presupposes the introduction of additional parameters as random variables, thereby increasing the computational complexity.

3. For the calibration curve, linearity is assumed. More complex relations between potential drop and crack size are conceivable, thereby allowing for other crack propagation geometries as well, albeit resulting in a higher dimensionality of the parameter vector and consequently the computational complexity.

4. The convergence behaviour mentioned in Enumeration 1. should be addressed with an increased measuring rate especially in the latter part of the stable crack growth stage, where the non-linearity of the crack propagation intensifies.

REFERENCES

[1] G. Sposito, Advances in potential drop techniques for non-destructive testing, Ph.D. thesis, Imperial College London (2009).

[2] T. Berg, S. von Ende, R. Lammering, Calibration of potential drop measuring and damage extent prediction by Bayesian filtering and smoothing, International Journal of Fatigue 100, 337–346, 2017. doi:10.1016/j.ijfatigue.2017.03.033.

[3] R. O. Ritchie, K. J. Bathe, On the calibration of the electrical potential technique for monitoring crack growth using finite element methods, International Journal of Fracture 15 (1), 47–55, 1979. doi:10.1007/BF00115908.

[4] K. George, H. Reemsnyder, J. Donald, R. Bucci, Development of a DCPD Calibration for Evaluation of Crack Growth in Corner-Notched, Open-Hole Specimens, Journal of ASTM International 1 (9), 19044, 2004. doi:10.1520/JAI19044.

[5] G. Belloni, E. Gariboldi, A. Lo Conte, M. Tono, P. Speranzoso, On the Experimental Calibration of a Potential Drop System for Crack Length Measurements in a Compact Tension Specimen, Journal of Testing and Evaluation 30 (6), 1–9, 2010. doi:10.1520/JTE12346J.

[6] C. Schweizer, M. Schlesinger, H. Oesterlin, V. Friedmann, P. Bednarz, C. Meilgen, J. Szwedowicz, Methodology for fatigue crack growth testing under large scale yielding conditions on corner-crack specimens, Engineering Fracture Mechanics 126, 126–140, 2014. doi:10.1016/j.engfracmech.2014.04.032.

[7] H. Johnsen, Calibrating the Electric Potential Method for Studying Slow Crack Growth, Materials Research & Standards 5, 442–445, 1965.

[8] R. A. Cláudio, C. M. Branco, J. Byrne, Numerical calibration of electric potential difference for crack size monitoring, in: 10th Portuguese Conference on Fracture, 2006.

[9] L. Doremus, Y. Nadot, G. Henaff, C. Mary, S. Pierret, Calibration of the potential drop method for monitoring small crack growth from surface anomalies Crack front marking technique and finite element simulations, International Journal of Fatigue 70, 178–185, 2015. doi:10.1016/j.ijfatigue.2014.09.003.

[10] A. M. Stuart, Inverse problems: A Bayesian perspective, Acta Numerica 19 (May 2010), 451–559, 2010. doi:10.1017/S0962492910000061.

[11] X. Guan, R. Jha, Y. Liu, Model selection, updating, and averaging for probabilistic fatigue damage prognosis, Structural Safety 33 (3), 242–249, 2011. doi:10.1016/j.strusafe.2011.03.006.

[12] M. Gobbato, J. B. Kosmatka, J. P. Conte, Developing an integrated structural health monitoring and damage prognosis (SHM-DP) framework for predicting the fatigue life of adhesively-bonded composite joints, in: Fatigue and Fracture of Adhesively-Bonded Composite Joints, Elsevier Ltd, 2014, pp. 493–526. doi:10.1016/B978-0-85709-806-1.00017-3.

[13] T. Sullivan, Introduction to Uncertainty Quantification, Vol. 63 of Texts in Applied Mathematics, Springer International Publishing, Cham, 2015. doi:10.1007/978-3-319-23395-6.

[14] M. Daigle, B. Saha, K. Goebel, A comparison of filter-based approaches for model-based prognostics, in: 2012 IEEE Aerospace Conference, IEEE, 2012, pp. 1–10. doi:10.1109/AERO.2012.6187363.

[15] S. Sankararaman, S. Mahadevan, Separating the contributions of variability and parameter uncertainty in probability distributions, Reliability Engineering and System Safety 112, 187–199, 2013. doi:10.1016/j.ress.2012.11.024.

[16] S. Sankararaman, Significance, interpretation, and quantification of uncertainty in prognostics and remaining useful life prediction, Mechanical Systems and Signal Processing 52-53 (1), 228–247, 2015. doi:10.1016/j.ymssp.2014.05.029.

[17] H. G. Matthies, A. Litvinenko, B. V. Rosić, E. Zander, Bayesian Parameter Estimation via Filtering and Functional Approximations (1), 1–30, 2016. arXiv:1611.09293.

[18] O. G. Ernst, B. Sprungk, H.-j. Starkloff, Bayesian Inverse Problems and Kalman Filters, Vol. 102, 2014, pp. 133–159. doi:10.1007/978-3-319-08159-5˙7.

[19] S. Sarkka, Bayesian Filtering and Smoothing, Cambridge University Press, Cambridge, 2013. doi:10.1017/CBO9781139344203.

[20] R. E. Kalman, A New Approach to Linear Filtering and Prediction Problems, Journal of Basic Engineering 82 (1), 35, 1960. doi:10.1115/1.3662552.

[21] H. E. Rauch, F. Tung, C. T. Striebel, Maximum likelihood estimates of linear dynamic systems, AIAA Journal 3 (8), 1445–1450, 1965. doi:10.2514/3.3166.

[22] M. Arulampalam, S. Maskell, N. Gordon, T. Clapp, A tutorial on particle filters for online nonlinear/non-Gaussian Bayesian tracking, IEEE Transactions on Signal Processing 50 (2), 174–188, 2002. doi:10.1109/78.978374.

[23] Z. H. E. Chen, Bayesian Filtering: From Kalman Filters to Particle Filters, and Beyond, Statistics 182 (1), 1–69, 2003.

[24] D. S. Kalogerias, A. P. Petropulu, Grid based nonlinear filtering revisited: Recursive estimation & asymptotic optimality, IEEE Transactions on Signal Processing 64 (16), 4244–4259, 2016. arXiv:1604.02631, doi:10.1109/TSP.2016.2557311.

[25] I. Arasaratnam, S. Haykin, Cubature Kalman Filters, IEEE Transactions on Automatic Control 54 (6), 1254–1269, 2009. doi:10.1109/TAC.2009.2019800.

[26] S. J. Julier, J. K. Uhlmann, New extension of the Kalman filter to nonlinear systems, in: I. Kadar (Ed.), Proc. of AeroSense: The 11the Int. Symp. on Aerospace/Defence Sensing, Simulation and Controls, 1997, p. 182. doi:10.1117/12.280797.

[27] E. a. Wan, R. Van Der Merwe, The unscented Kalman filter for nonlinear estimation, Technology v, 153–158, 2000. doi:10.1109/ASSPCC.2000.882463.

[28] S. Julier, J. Uhlmann, Unscented Filtering and Nonlinear Estimation, Proceedings of the IEEE 92 (3), 401–422, 2004. doi:10.1109/JPROC.2003.823141.

[29] J. Kokkala, A. Solin, S. Särkkä, Sigma-Point Filtering and Smoothing Based Parameter Estimation in Nonlinear Dynamic Systems (1), 1–11, 2015. arXiv:1504.06173.

[30] N. Perez, Fracture Mechanics, Vol. 1, Kluwer Academic Publishers, Boston, 2004. doi:10.1007/b118073.

[31] L. Zhao, J. Tong, J. Byrne, Stress intensity factor K and the elastic T-stress for corner cracks, International Journal of Fracture 109 (2), 209–225, 2001. doi:10.1023/A:1011016720630.

[32] M. Schlesinger, C. Schweizer, Y. Brontfeyn, H. Oesterlin, Experimental investigation of the thermomechanical fatigue crack growth and theoretical description by the effective cyclic crack tip opening displacement, in: DGM Conference on material testing, 2013.

[33] P. Paris, F. Erdogan, A Critical Analysis of Crack Propagation Laws, Journal of Basic Engineering 85 (4), 528–533, 1963. doi:10.1115/1.3656900.

[34] R. Ritchie, Mechanisms of Fatigue-Crack Propagation in Ductile and Brittle Solids, International Journal of Fracture 100, 55–83, 1999. arXiv:0005074v1, doi:10.1023/A:1018655917051.

[35] A. C. Pickard, The application of 3-dimensional finite element methods to fracture mechanics and fatigue life prediction, Engineering Materials Advisory Services Limited, 1986.

[36] D. Broek, Fatigue crack propagation, in: Elementary engineering fracture mechanics, Vol. 166, Springer Netherlands, Dordrecht, 1982, pp. 250–287. doi:10.1007/978-94-009-4333-9˙10.

[37] K. Walker, The Effect of Stress Ratio During Crack Propagation and Fatigue for 2024-T3 and 7075-T6 Aluminum, in: Effects of Environment and Complex Load History on Fatigue Life, ASTM International, 100 Barr Harbor Drive, PO Box C700, West Conshohocken, PA 19428-2959, 1970, pp. 1–1–14. doi:10.1520/STP32032S.

[38] R. G. Forman, V. E. Kearney, R. M. Engle, Numerical Analysis of Crack Propagation in Cyclic-Loaded Structures, Journal of Basic Engineering 89 (3), 459–463, 1967. doi:10.1115/1.3609637.

[39] D. Broek, J. Schijve, The Influence of the Mean Stress on the Propagation of Fatigue Cracks in Light Alloy Sheet, Aircraft Engineering and Aerospace Technology 39 (3), 10–18, 1967. doi:10.1108/eb034240.

[40] A. Hartman, J. Schijve, The effects of environment and load frequency on the crack propagation law for macro fatigue crack growth in aluminium alloys, Engineering Fracture Mechanics 1 (4), 615–631, 1970. doi:10.1016/0013-7944(70)90003-2.

[41] R. G. Forman, S. R. Mettu, Behavior of surface and corner cracks subjected to tensile and bending loads in a Ti-6Al-4V alloy, Fracture Mechanics: Twenty-second Symposium I, 519–546, 1992.

[42] J. Maierhofer, R. Pippan, H. P. Gänser, Modified NASGRO equation for physically short cracks, International Journal of Fatigue 59, 200–207, 2014. doi:10.1016/j.ijfatigue.2013.08.019.

[43] A. Papavasiliou, Parameter estimation and asymptotic stability in stochastic filtering, Stochastic Processes and their Applications 116 (7), 1048–1065, 2006. doi:10.1016/j.spa.2006.01.002.

[44] N. Chopin, P. E. Jacob, O. Papaspiliopoulos, SMC 2 : an efficient algorithm for sequential analysis of state space models, Journal of the Royal Statistical Society: Series B (Statistical Methodology) 75 (3), 397–426, 2013. arXiv:1101.1528, doi:10.1111/j.1467-9868.2012.01046.x.

[45] D. Crisan, J. Miguez, Nested particle filters for online parameter estimation in discrete-time state-space Markov models, arXiv.org stat.CO, 1–48, 2016. arXiv:1308.1883.